Collective stop-and-go dynamics of active bacteria swarms

Daniel Svenšek[1],* Harald Pleiner[2], and Helmut R. Brand[3]
[1] *Department of Physics, Faculty of Mathematics and Physics, University of Ljubljana, SI-1000 Ljubljana, Slovenia*
[2] *Max-Planck-Institute for Polymer Research, POBox 3148, 55021 Mainz, Germany*
[3] *Theoretische Physik III, Universität Bayreuth, 95440 Bayreuth, Germany*
(Received 1 March 2013; revised manuscript received 22 September 2013; published 25 November 2013)

We set up a macroscopic model of bacterial growth and transport based on a dynamic preferred direction – the collective velocity of the bacteria. This collective velocity is subject to the isotropic-nematic transition modeling the density-controlled transformation between immotile and motile bacterial states. The choice of the dynamic preferred direction introduces a distinctive coupling of orientational ordering and transport not encountered otherwise. The approach can be applied also to other systems spontaneously switching between individual (disordered) and collective (ordered) behavior, and/or collectively responding to density variations, e.g., bird flocks, fish schools etc. We observe a characteristic and robust stop-and-go behavior. Inclusion of chirality results in a complex pulsating dynamics.

DOI: 10.1103/PhysRevLett.111.228101 PACS numbers: 87.18.Hf, 47.63.Gd, 05.70.Ln, 61.30.-v

For biological systems the description of the collective motion of self-propelled units giving rise to a large number of spatio-temporal patterns is one of the central questions. From a physical point of view the complexity of biological or active systems on macroscopic and mesoscopic scales represents a large class of driven nonequilibrium systems. Collective behavior arises on many different length and time scales including the large scale spatio-temporal patterns of bird flocks and fish schools [1–6], the intermediate size spatio-temporal complexity revealed by various types of bacteria [7–15] as well as the mesoscopic collective motion shown by microscopic motors [16–21].

To describe these collective phenomena frequently reaction-diffusion type models for the various concentrations of species involved have been used. Naturally an important issue arises, namely the question whether there are other macroscopic variables of interest. Correspondingly the use of modified nematodynamic equations to describe active systems including nonpolar [22] as well as polar [23] has been advocated. Another approach suggests the use of dynamic preferred directions [24, 25]. For example, the preferred direction in a bird flock or a swarm of insects is certainly dynamic and does not exist statically. As we will argue below a polar dynamic preferred direction arises naturally as a macroscopic variable to describe the spatio-temporal patterns revealed by certain types of bacteria. This unconventional choice introduces a distinctive coupling of orientational ordering and transport not encountered in the case of the static preferred direction. We think that with its natural application also to other systems it could become generic.

In the present Letter we suggest and analyze a model to capture various aspects of the experimental results described by Matsushita's group for the bacterium *Proteus mirabilis* [11–15]. Especially our model covers various features of the intricate collective dynamics shown by *Proteus mirabilis* including in particular a pulsating dynamics of a collective stop-and-go type presented in detail in Ref. [13], where it is confirmed that the pulsing is not due to biological (internal clock of the bacteria) or chemical (chemotaxis) factors.

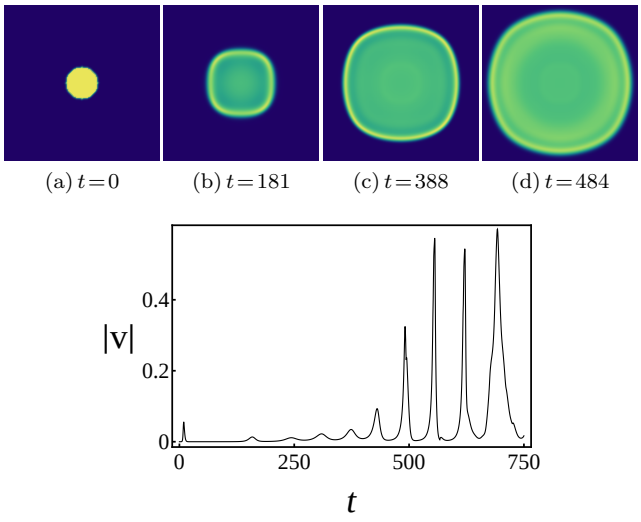

FIG. 1. (color online) Top: Growth of the colony after the "point" inoculation with $\rho = 0.2$: density snapshots (bright regions represent high density) of achiral population (a-d). Bottom: the time dependence of the sample-average magnitude of the velocity demonstrates the step-like growth dynamics, which is best seen in the supplemental movies.

The variables of the model are the density of the nutrient (food) f, the density of the bacteria ρ, and their macroscopic velocity $\mathbf{v}$. Food is considered immobile and

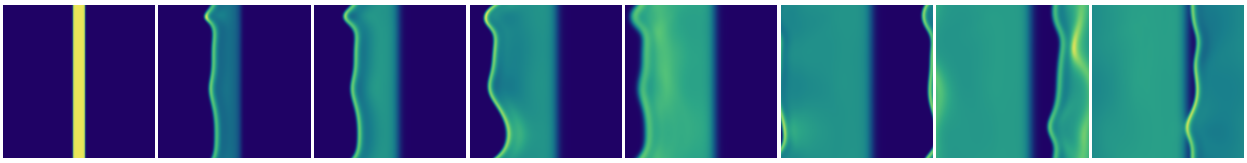

(a) $t=0$ (b) $t=25$ (c) $t=137$ (d) $t=204$ (e) $t=275$ (f) $t=289$ (g) $t=375$ (h) $t=388$

FIG. 2. Density snapshots (bright represents high density) (compare with Fig. 3a) of the growing colony after a slightly randomly perturbed line inoculation with $\rho = 0.2$ (a). Due to the periodic boundary conditions, in (f) the front, after passing the left boundary, reenters the system from the right. Note the internal waves in (e) and (g) advancing towards the front and pushing it ahead afterwards. In (h) the whole system is about to be populated; subsequently the front moves continuously.

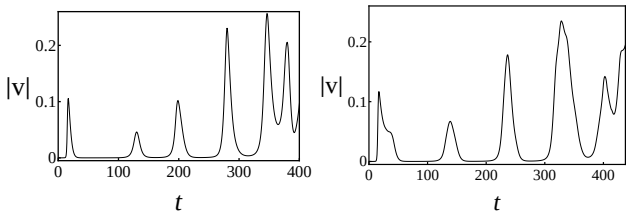

(a) achiral (b) chiral

FIG. 3. Growth of the colony after the perturbed line inoculation: the time dependence of the sample-average magnitude of the velocity demonstrates clear-cut pulses and almost no dynamics between them; (a) no chirality and (b) $K_c = 0.0034$.

is thus only consumed by the bacteria,

$$\dot{f} = -\alpha\,\rho\,\tilde{f}, \tag{1}$$

where $\dot{f} = \partial f/\partial t$, α is a coefficient determining the rate of food consumption, and $\tilde{f} = f/(f^{sat}+f)$ is a saturated nutrient density preventing overconsumption, if food is in excess with respect to a saturation density f^{sat}.

The dynamic equation for the bacterial density takes into account the growth due to food consumption as well as advective and diffusive transport (the latter mainly for smoothing):

$$\frac{\partial \rho}{\partial t} + v_0 \nabla\cdot(\rho\,\mathbf{b}) + \nabla\cdot\mathbf{j}_D = -\dot{f}\ \frac{\rho^{sat}-\rho}{\rho^{sat}}, \tag{2}$$

where $\mathbf{b}$ is the velocity order parameter, v_0 sets the physical velocity scale, $\mathbf{v} = v_0\mathbf{b}$, and $\mathbf{j}_D = -D\nabla\rho$. The stabilizing factor on the right prevents possible uncontrolled growth of the density above a saturation density ρ^{sat}.

The transformation between the vegetative (essentially immotile) and the motile swarmer cells is modeled by the analog of the isotropic-nematic (I-N) transition of the velocity order parameter (similar in spirit to [24]) controlled by the rate of food consumption $\dot{f}$ (depending only on ρ if food is abundant):

$$\gamma\left[\frac{\partial \mathbf{b}}{\partial t} + v_0(\mathbf{b}\cdot\nabla)\mathbf{b}\right] = [A(|\dot{f}| - |\dot{f}^*|) - Cb^2]\mathbf{b} + L\nabla^2\mathbf{b} - K_p\nabla\rho + K_f\nabla\tilde{f} + K_c\mathbf{p}\times\mathbf{b}, \tag{3}$$

where γ, the analog of the nematic rotational viscosity, defines the time scale of the velocity field, A and C are the Landau coefficients of the I-N phase transition, $|\dot{f}^*| = \alpha\tilde{f}\rho^*$ is the transition threshold (ρ^* is the local threshold density), and L is the analog of a nematic elastic constant. The K_p term – analog of the pressure term in the Navier-Stokes equation – prevents a possible build-up of too strong sources and sinks in our highly compressible bacterial "fluid". Here we assumed a "compressibility" relation $d\rho = dp/K_p$. The K_f coupling mimics the tendency of the bacteria to orient themselves and move along the food gradient. And finally, the K_c term representing the lowest order chiral coupling that is allowed by symmetry, describes the left-right asymmetry, i.e. the preference of the bacteria to turn left or right while moving, depending on the sign of K_c; $\mathbf{p}$ is the substrate normal.

In this study, we focus on the expanding growth phase of the bacterial colony. Starting with an unpopulated nutrient-rich surface, we inoculate a finite bacterial density ρ in the center of the domain. Using periodic boundary conditions we let the colony evolve until it touches itself after passing the domain boundary. Time, length and density units may be chosen such that, e.g., $\alpha = L = \rho^* = 1$. Yet for clarity, we do not introduce any dimensionless quantities at this stage. As a starting point, the following numerical values of the parameters (in arbitrary units) will be used unless stated otherwise: $A = 100$, $C = 1$, $L = 0.1$, $v_0 = 5$, $|\dot{f}^*| = 0.001$, $\alpha = 0.012$, $f^{sat} = 0.5$, $\rho^{sat} = 0.2$, $D = 0.01$, $K_p = 10^{-6}$, $K_f = 0.01$, $K_c = 0$, and $1/\gamma = 18$. The initial density of the nutrient will be $f = 5$, which is already in the excess regime for the examples presented, for which f is thus not a decisive variable. Following the experiment we nevertheless keep it as a part of our model to take into account the decreasing activity on longer time scales. The system size is 60×60, calculated on a 142×142 mesh. The consistency of the results was checked for larger meshes as well.

First we show a circularly symmetric "point" nucleation of achiral bacteria, which demonstrates a symmetrical growth, Fig. 1a-d, with an interesting stop-and-go behavior of the colony front (see Supplemental Material

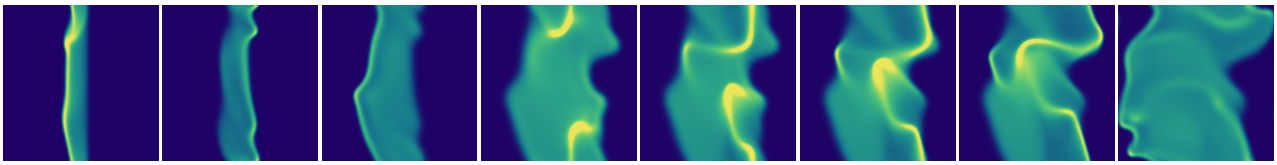

(a) $t=21$ (b) $t=49$ (c) $t=156$ (d) $t=320$ (e) $t=325$ (f) $t=329$ (g) $t=334$ (h) $t=371$

FIG. 4. (color online) Density snapshots (bright represents high density) (compare with Fig. 3b) of the growing colony after a slightly randomly perturbed line inoculation (the same as in Fig. 2a) in a chiral system with $K_c = 0.0034$ (compare Fig. 6f to locate it in the chirality diagram). (a-c) The front typically moves back and forth across the populated region. (d-g) Two fronts are interestingly passing next to each other. (h) The last calm stage before the whole system gets populated.

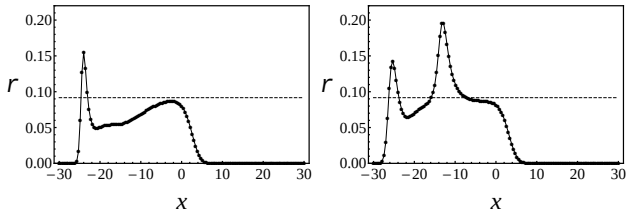

(a) reposing phase (b) active phase

FIG. 5. Density profile snapshots (horizontal central cross sections of density fields like in Fig. 2): (a) reposing phase with the static front (the peak on the left) and (b) active phase showing an internal density wave travelling towards the front. The threshold density ρ^* is shown dashed.

at [URL will be inserted by publisher] for the movies). To what extent such a stop-and-go behavior is pronounced depends on the material parameters, but it turns out to be a general feature of the model. It emerges that the periodic growth dynamics corresponds to experimental observations [13]. Furthermore, in the same paper Matsushita *et al.* also report on one or more internal waves that are observed to advance towards the growth front. Our results also exhibit such waves [26].

The pulsing can be quantified by plotting the time evolution of the norm of the velocity field, e.g., the average magnitude of the velocity field, Fig. 1(bottom), which is a good measure of the velocity of the growth front. The phases of cessation and activation are related to the I-N transition of the velocity field mimicking the density-controlled transition between vegetative and swarmer cells.

For analytic purposes we inoculate the colony in a straight line, Fig. 2, and slightly perturb it randomly to avoid any symmetry induced degeneracy. A left-right symmetric growth is typically unstable and the growth to one side usually dominates. Despite its wrinkledness, the front advances in clear-cut pulses, as demonstrated in Fig. 3. This remains true even in the chiral case, Figs. 3b and 4. Although the front gets distorted and exhibits spatially more complicated dynamics, the pulses and the calm periods nevertheless persist. A remarkable general feature of these pulsating processes is the clear distinction of active and reposing phases (note the almost complete stopping between the pulses) – a continuous system that exhibits a rather distinct discrete dynamics.

In the growing colony the density front is always formed, even if the system is initially homogeneous. In Eqs. (4)-(6) we will assume $\tilde{f} = 1$. When ρ is sufficiently above the threshold density ρ^*, the homogeneous state becomes linearly unstable against any velocity perturbation with a nonzero wavenumber k, which according to Eq. (3) grows at a rate

$$1/\tau_v = \frac{1}{\gamma}\left[A\alpha(\rho-\rho^*) - Lk^2\right] \tag{4}$$

and triggers the density instability via compressible flow (the second term of Eq. (2)).

A cross section through the front, Fig. 5, reveals its structure and a qualitative mechanism of repose and activity. The density peak of the front is always above the threshold and the velocity there is held close to zero by the elasticity, Fig. 5a; the width of the front is proportional to the correlation length of the velocity field, $\xi_L = \sqrt{L/A\alpha(\rho-\rho^*)}$. As the bacteria grow the density of the interior region gradually increases. When sufficiently above the threshold, a travelling pulse is usually triggered from this region by the above instability, Fig. 5b. It passes through the original front and finally comes to rest forming the new static front. Sometimes there is no internal excitation but merely the original front that starts moving again. Governed by the growth, the duration of the reposing phase and thus the time interval between the pulses scales with $\tau_\rho = 1/\alpha$.

In the active phase, advection is dominant and one can approximately neglect growth and diffusion in Eq. (2). In one dimension, the resulting continuity equation for the bacterial density can be rewritten requiring $d\rho = 0$:

$$\frac{dx}{dt} = \frac{d(\rho v)}{d\rho} = v + \rho\frac{dv}{d\rho}, \quad \rho = \text{const}, \tag{5}$$

where dx/dt is thus the speed of the observer following constant density. In the limit of small γ, one can further

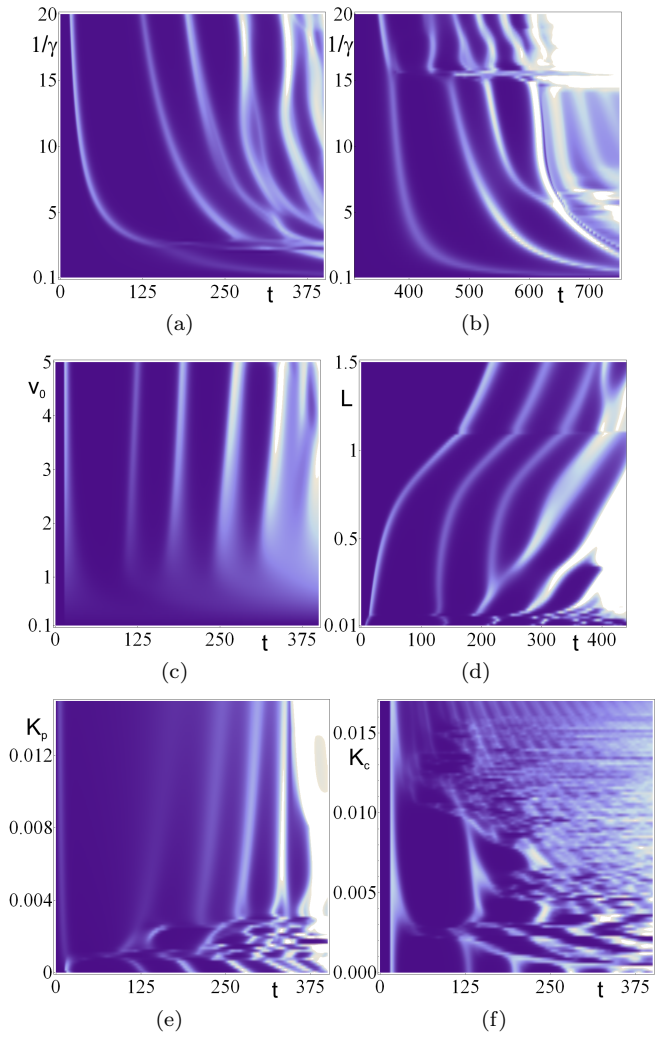

FIG. 6. (color online) "Dynamograms" showing the growth dynamics morphology (bright regions represent active stages) as a function of time (horizontal axis) and the model parameters (vertical axis). (a, b) Dependence on $1/\gamma$, the responsiveness of the velocity field, for two values of the inoculation density, $\rho = 0.2$ (a) and $\rho = 0.02$ (b); note the time shift in (b). (c) Dependence on the velocity scale v_0, (d) dependence on L, (e) the role of compressibility, and (f) the influence of chirality. Late stages (shown partially) exhibit an increased activity after the whole area has been populated. Taking horizontal cross sections produces velocity profiles like in Fig. 3.

assume that $v = v(\rho) = v_0\sqrt{\alpha A(\rho - \rho^*)/C}$, and hence

$$\frac{dx}{dt} = v(\rho) + \frac{\alpha A v_0^2}{2C}\rho\frac{1}{v(\rho)}. \qquad (6)$$

Due to the critical behavior of the second term, the density values just above the threshold ρ^* are transported rapidly – this explains the onset of the density waves propagating from the interior towards the front. High density peaks are transported with the velocity close to

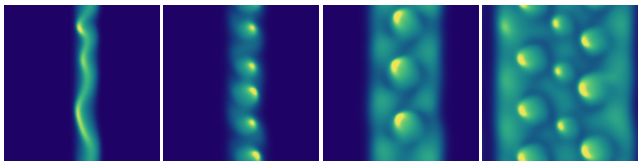

(a) $t = 50$ (b) $t = 220$ (c) $t = 644$ (d) $t = 1240$

FIG. 7. Snapshots of the self-organization into a slowly expanding rotation lattice for a larger chirality parameter $K_c = 0.03$ (bright represents high density). (a) Initially the front is moving back and forth across the populated region and becomes unstable along its length, forming the rotation cells in (b). Then the colony is slowly expanding by diffusion and growth (c, d) and new rotation cells "ignite" gradually (upper left part of (d)) when the bacterial density increases. In all the cells the front (seen as the bright patch) undergoes a synchronous, phase-locked rotation. When a new set of cells appears at the edge of the colony, the inner cells shrink in size.

that of the fluid, $v(\rho)$, as $dv/d\rho$ in Eq. (5) gets small with increasing density. A special density value is related to the extremum of the velocity (6), which is lowest for $\rho = 2\rho^*$, defining ρ^* as the relevant density scale also above the threshold. We note that the density peaks of the front are all close to this value quite irrespective of the parameters including also ρ^{sat}. Moreover, for the colony that is expanding into an unpopulated region the density saturation does not have any qualitative influence and can be omitted.

In what follows, we study the influence of the model parameters on the pulsating dynamics to shed light on the pulsating region of the parameter space. We perform scans of the dynamic profiles like the one in Fig. 3, varying one model parameter at a time. The result are two-dimensional "dynamograms", Fig. 6, the horizontal cross section of which corresponds to the dynamic profile of activity and repose, while its dependence on the model parameter is presented along the vertical axis. Unless stated otherwise, the initial condition is the same as in Fig. 2. For comparability we use the same random sequence for the initial perturbation in all cases, while we verified that the dynamograms are virtually identical for other sequences.

Fig. 6a shows that the pulsing is weakened by decreasing the responsiveness $1/\gamma$ of the velocity and eventually almost vanishes. For a weaker inoculation, Fig. 6b, it is demonstrated that the pulsating dynamics is still there, after the initial population has grown to the threshold level. It is thus not a peculiarity of the initial condition. The velocity magnitude v_0, Fig. 6c, has almost no influence on the timing of the pulses, yet they gradually disappear with decreasing v_0. Fig. 6d confirms that the morphology of the dynamics depends on the correlation length ξ_L, which increases with increasing L.

It turns out that the compressibility of the bacterial

"fluid" is essential for the stop-and-go dynamics, which is in accord with the experimental evidence supporting the importance of local density variations in this context [13]. At higher values of K_p the pulsing gets strongly suppressed, as demonstrated in Fig. 6e, which also shows that the value $K_p = 10^{-6}$ we have used throughout this study is practically zero and fits into the region where the pulsing is most pronounced.

In all of the presented examples the density of the nutrient is in excess, therefore the influence of the K_f parameter is only minor and will not be presented. We recall that in this regime the actual control parameter of the I-N transition in Eq. (3) is the density ρ, Eq. (1), which is the standard control candidate in many systems ranging from lyotropic liquid crystals to flocking animals.

As already observed for the chiral system presented in Fig. 4, it is confirmed by the dynamogram in Fig. 6f that the pulsing is retained for moderate values of K_c. On the other hand, in the region of higher K_c, appearing as faint regular stripes in Fig. 6f, the pulsating dynamics of the front is replaced by a local circular motion, which is self-organized into a regular lattice of rotation cells (see Supplemental Material [27]). This phenomenon has not yet been observed experimentally and thus presents a prediction which can be tested in future experiments.

The model has potential applications also for various other systems, in particular for flocking animals like insects, birds, and fish. While tailored and fine-tuned to the specific situation, the coupling between orientational ordering and transport remains its distinct feature. In the case of birds or fish, for example, one would omit Eq. (1) and the growth term in Eq. (2), include an 'interfacial' tension characteristic for flocking, and set up a suitable coupling between density gradients and velocity to model the sudden yet collective direction changes typical for bird flocks or fish schools: birds do not stop when flying, but they react to density changes by changing the flight direction. Recent experimental studies have reached a number of several thousand birds [5, 6], finally enabling three dimensional continuum studies of these systems.

It is a pleasure to thank Mitsugu Matsushita for many discussions about his experimental results. D.S. acknowledges the support of the Agency for Research and Development of Slovenia (Grants No. J1-4297, J1-4134).

* corresponding author: daniel.svensek@fmf.uni-lj.si

[1] Y. Katz, K. Tunstrom, C. C. Ioannou, C. Huepe, I. Couzin, *Proc. Natl. Acad. Sci. U.S.A.* **108**, 18720 (2011).

[2] J. Buhl, D. J. T. Sumpter, I. D. Couzin, J. J. Hale, U. Despland, E. R. Miller, S. J. Simpson, *Science* **312**, 1402 (2006).

[3] R. Lukeman, Y. Li, L. Edelstein-Keshet, *Proc. Natl. Acad. Sci. U.S.A.* **107**, 12576 (2010).

[4] J.K. Parrish and L. Edelstein-Keshet, *Science* **284**, 99 (1999).

[5] M. Ballerini, N. Cabibbo, R. Candelier, A. Cavagna, E. Cisbani, I. Giardina, V. Lecomte, A. Orlandi, G. Parisi, A. Procaccini, M. Viale, V. Zdravkovic, *Proc. Natl. Acad. Sci. U.S.A.* **105**, 1232 (2008).

[6] M. Ballerini, N. Cabibbo, R. Candelier, A. Cavagna, E. Cisbani, I. Giardina, A. Orlandi, G. Parisi, A. Procaccini, M. Viale, V. Zdravkovic, *Animal Behaviour* **76**, 201 (2008).

[7] L. Cisneros, R. Cortez, C. Dombrovski, R. Goldstein, J. Kessler, *Exp. Fluids* **43**, 737 (2007).

[8] M. Loose, E. Fischer-Friedrich, J. Ries, K. Kruse, P. Schwille, *Science* **320**, 789 (2008.)

[9] H. P. Zhang, A. Be'er, E.-L. Florin, H. L. Swinney, *Proc. Natl. Acad. Sci. U.S.A.* **107**, 13626 (2010).

[10] X. Fu, L. H. Tang, C. Liu, J. D. Huang, T. Hwa, P. Lenz, *Phys. Rev. Lett* **108**, 198102 (2012).

[11] K. Watanabe, J. Wakita, H. Itoh, H. Shimada, S. Kurosu, T. Ikeda, Y. Yamazaki, T. Matsuyama, M. Matsushita, *J. Phys. Soc. Jpn.* **71**, 650 (2002).

[12] O. Moriyama, M. Matsushita, *J. Phys. Soc. Jpn.* **64**, 1081 (1995).

[13] Y. Yamazaki, T. Ikeda, H. Shimada, F. Hiramatsu, N. Kobayashi, J. Wakita, H. Itoh, S. Kurosu, M. Nakatsuchi, T. Matsuyama, M. Matsushita, *Physica* D **205**, 136 (2005).

[14] M. Matsushita, J. Wakita, H. Itoh, K. Watanabe, T. Arai, T. Matsuyama, H. Sakaguchi, M. Mimura, *Physica* A **274**, 190 (1999).

[15] M. Matsushita, J. Wakita, H. Itoh, I. Ràfols, T. Matsuyama, H. Sakaguchi, M. Mimura, *Physica* A **249**, 517 (1998).

[16] V. Schaller, C. Weber, C. Semmrich, E. Frey, A. R. Bausch, *Nature* **467**, 73 (2010).

[17] V. Schaller, C. A. Weber, B. Hammerich, E. Frey, A. R. Bausch, *Proc. Natl. Acad. Sci. U.S.A.* **108**, 19183 (2011).

[18] R. A. Simha, S. Ramaswamy, *Phys. Rev. Lett.* **89**, 058101 (2002).

[19] Y. Hatwalne, S. Ramaswamy, M. Rao, R. A. Simha, *Phys. Rev. Lett.* **92**, 118101 (2004).

[20] T. Surrey, F. Nédélec, S. Leibler, E. Karsenti, *Science* **292**, 1167 (2001).

[21] F. Nédélec, T. Surrey, A. C. Maggs, S. Leibler, *Nature* **389**, 305 (1997).

[22] K. Kruse. J.F. Joanny, F. Julicher, J. Prost, K. Sekimoto, *Eur. Phys. J.* E **16**, 5 (2005).

[23] S. Muhuri, M. Rao, and S. Ramaswamy, *EPL* **78**, 48002 (2007).

[24] T. Vicsek, A. Czirók, E. Ben-Jacob, I. Cohen, O. Shochet, *Phys. Rev. Lett.* **75**, 1226 (1995).

[25] H.R. Brand, H. Pleiner, D. Svenšek, *Eur. Phys. J.* E **43**, 128 (2011).

[26] See Supplemental Material at http://link.aps.org/supplemental/10.1103/PhysRevLett.111.228101 for the movies corresponding to Figs. 1, 2, 4, and 5.

[27] See Supplemental Material at http://link.aps.org/supplemental/10.1103/PhysRevLett.111.228101 for the movie *rotation_lattice.mpg* showing the self-organization into a slowly expanding rotation lattice for $K_c = 0.03$.